16

A Review of Indoor Localization Methods Based on Inertial Sensors

Estefania Munoz Diaz, Dina Bousdar Ahmed, Susanna Kaiser

INSTITUTE OF COMMUNICATIONS AND NAVIGATION, GERMAN AEROSPACE CENTER (DLR), OBERPFAFFENHOFEN, GERMANY

1 Introduction

Different solutions exist to solve the pedestrian indoor localization problem, but many of them rely on additional infrastructure that either needs to be installed or is assumed to be available. An overview of different techniques that address the challenges in areas not covered by Global Navigation Satellite Systems (GNSS) is given in Liu et al. (2007), Gu et al. (2009), and Harle (2013).

Radio and satellite navigation solve the positioning problem using the piloting method. Piloting is the process of determining one's position based on external objects, such as antennas or satellites. Inertial navigation performs positioning using the dead-reckoning method. Dead-reckoning is the process of determining one's current position projecting course and speed or elapsed distance from a known previous position. Dead-reckoning is, therefore an infrastructure-free positioning system.

Pedestrian dead-reckoning is performed using inertial sensors that are usually combined with magnetometer and barometer. Inertial sensors are of high interest because of the possibility of providing positioning without touching privacy, unlike camera-based systems. Since medium- or low-cost inertial sensors are already available in every smartphone or other carry on electronic devices, the use of inertial sensors is especially interesting for mass market applications.

Example application areas suitable for inertial positioning are fire fighter rescuing, police men supervision, industrial inspections, or supervision of elderly people. Those professional applications require a system that is small-sized, light-weighted, has low power consumption, can be easily mounted on the body and is not dependent on infrastructure. For instance, in the case of fire, infrastructure might be disturbed. In addition, in some applications cameras might not be allowed as it is the case in industrial inspections. Integrating inertial sensors in clothes or footwear is an option to handle the fixation of sensors.

Geographical and Fingerprinting Data for Positioning and Navigation Systems. https://doi.org/10.1016/B978-0-12-813189-3.00016-2

Suited sensor locations are the shoe or the pocket (Munoz Diaz et al., 2014; Bousdar et al., 2016). Alternatively, sensor locations mounted, e.g., at the wrist (Diez et al., 2016), at the head (Windau and Itti, 2016), at the torso (Do et al., 2016), or in the backpack are also investigated. Nevertheless, it is still challenging to use the sensors of the smartphones for positioning without any other help due the fact that the sensor is usually not fixed at the body and is in different motion mode like texting, phoning, swinging, or even in irregular motion mode (Renaudin et al., 2012).

Besides using only inertial sensors, fusion with other sensors or maps of the environment (Beauregard et al., 2008; Krach and Robertson, 2008; Woodman and Harle, 2008; Kaiser et al., 2015) is in any case possible and recommendable. Additionally, the combination of sensors mounted on different locations of the human body is a promising solution for professional use cases (Bousdar et al., 2016).

In Section 2, inertial sensors as well as magnetometer sensors are explained. Pedestrian positioning systems based on inertial sensors are usually classified depending on the location of the body where they are mounted on. This classification is based on the algorithm they use to compute the position of the pedestrian. There are two types of algorithms, namely strapdown and step&heading. These two algorithms correspond with shoe-mounted positioning systems and non-shoe-mounted positioning systems, respectively. The estimation of the orientation is of key importance to perform inertial positioning and it is computed disregarding the location where the sensor is mounted on. Therefore, the orientation estimation is deeply described in Section 3, followed by the shoe-mounted inertial positioning in Section 4 and the non-shoe-mounted inertial positioning in Section 5. The positioning estimation based on medium- and low-cost inertial sensors suffers from propagation of errors and accumulated drift over time. Therefore, additional algorithms are necessary to compensate the drift. An extensive state of the art review is handled in Section 6. Finally, Section 7 is devoted to discussion of the present and future status of inertial positioning for pedestrians.

2 Inertial Sensors and Magnetometers

Inertial sensors are composed of accelerometers and gyroscopes, which measure specific force and turn rate, respectively. The so-called inertial measurement unit contains three mutually orthogonal accelerometers and three mutually orthogonal gyroscopes. Therefore, the acceleration and turn rate measurements are triads.

Inertial sensors based on micro-electromechanical (MEMS) technology have improved its performance over the last decades. However, using MEMS-based inertial sensors the resulting positioning is less accurate than using other technologies like solid state accelerometers or optical gyroscopes (Woodman, 2007). The most common error sources that disturb inertial measurements are biases, bias stability, and thermo-mechanical noise (Woodman, 2007).

The biases are the measured averaged value of the acceleration and turn rate when neither acceleration nor rotation, respectively, is undergoing. The biases introduce a systematic error in the integrated measurements, i.e., velocity, position, and orientation. The systematic error can be compensated by averaging acceleration and turn rate while the sensor is static and subtracting the averaged value from the measured acceleration and turn rate, respectively.

The bias stability describes how the biases change over time under stable conditions, usually at constant temperature. Temperature fluctuations due to changes in the environment and sensor self-heating modify the biases value. The change in the biases is caused by flicker noise, which is visible at low frequencies. Other slow changing errors also affect the bias values. The bias stability introduces a non systematic error in the integrated signals due to the fact that the biases wander over time.

The thermo-mechanical noise introduces a white noise sequence, namely a sequence of zero-mean uncorrelated random variables. In turn, such a sequence disturbs the integrated measurements, i.e., velocity, position, and orientation, by a random walk. A random walk is a process consisting of a series of steps, the direction and size of which are randomly determined (Woodman, 2007).

Magnetometers, which are commonly embedded together with the inertial sensors, measure magnetic fields, e.g., the Earth's magnetic field. Usually, a magnetometer unit is formed by three mutually orthogonal magnetometers. MEMS-based magnetometers are frequently found in smartphones and similar electronic devices. Nevertheless, other technologies exist to implement magnetic field sensors (Lenz and Edelstein, 2006).

The main phenomenon that affects the performance of magnetic field sensors is the temperature effect. The temperature error causes an increasing noise present in the measured magnetic field. Therefore, temperature compensation algorithms or specific electronic design (Beroulle et al., 2003) are required to limit the temperature effect.

For navigation purposes the Earth's magnetic field is widespread used. However, magnetometers are also affected by the presence of ferromagnetic materials, which are common in urban and indoor environments. The modifications introduced by these materials lead to erroneous orientation estimation. This is the reason why magnetic field sensors are historically ruled out from indoor navigation systems. Nevertheless, magnetometers can still be used to improve the performance of inertial sensors (Azfal et al., 2011; Zampella et al., 2012; Munoz Diaz et al., 2017).

3 Orientation Estimation

The orientation estimation aims at combining the measurements of gyroscopes, accelerometers, and magnetometers in an optimal way to obtain the orientation of the sensor. Along with the orientation angles, it is convenient to estimate also the biases of the gyroscopes. The biases, which were explained in Section 2, are therefore estimated in order to be subtracted from the turn rate measurements.

A common tool to compute the orientation in the state of the art is the Kalman filter. A Kalman filter is one implementation of Bayesian filters used to estimate the states of a system. In the particular case of the orientation estimation the states are the orientation angles, i.e., ϕ roll, θ pitch, and ψ yaw or heading, and the biases of the gyroscope.

The Kalman filter combines a prediction stage and an update stage. The prediction stage implements the system model, which represents how the system states evolve over time. The update stage incorporates measurements that relate to the system states. Usually the prediction stage is based on the integration over time of the turn rate measurements. The update stage typically incorporates the acceleration and magnetic measurements in order to reduce the error due to the integration over time of the turn rate measurements that contain biases and noise.

Both, the full state and the error state Kalman filter have similar performance, as shown in Wagner and Wieneke (2003). In this chapter, the full state vector is chosen, being $\boldsymbol{x}_{\mathrm{o}}^{k}$ composed of the orientation angles and the biases $\boldsymbol{b}^{k}$ of the gyroscopes:

$$\boldsymbol{x}_{\mathrm{o}}^{k} = [\phi^{k}, \theta^{k}, \psi^{k}, b_{\mathrm{x}}^{k}, b_{\mathrm{y}}^{k}, b_{\mathrm{z}}^{k}]^{T}. \tag{1}$$

In the following, α, ω, μ will be used to represent acceleration, turn rate, and magnetic measurements, respectively.

3.1 Prediction Stage

Gyroscopes measure in body frame the turn rate of the sensor with respect to the inertial frame. In order to have the turn rate measurements in body frame with respect to the navigation frame, the transport rate and the Earth rotation have to be subtracted. However, for pedestrian positioning, the transport rate is negligible and the Earth rotation, which is approximately $15^{\circ}\,\mathrm{h}^{-1}$, is usually not compensated. Therefore, it is assumed that the turn rate measured by the gyroscopes is approximately the turn rate of the sensor in body frame with respect to the navigation frame (see Fig. 1).

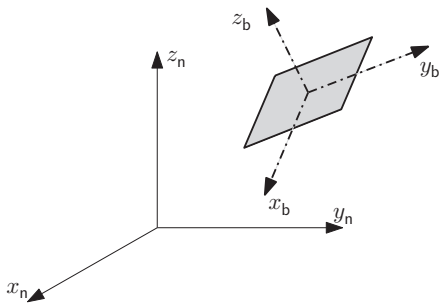

FIG. 1 Navigation frame, $\{\mathrm{x}, \mathrm{y}, \mathrm{z}\}_{\mathrm{n}}$, and body frame of the sensor, $\{\mathrm{x}, \mathrm{y}, \mathrm{z}\}_{\mathrm{b}}$. The navigation frame is fixed over time. The body frame changes with the sensor orientation.

The turn rate at the time k is defined as $\boldsymbol{\omega}^k = [\omega_x^k, \omega_y^k, \omega_z^k]^T$. To compute the orientation, the biases have to be subtracted from the turn rate. Then, the corrected turn rate measurements are integrated once over time.

The direction cosine matrix $\boldsymbol{C}^k$ is a 3×3 matrix in which each column is a unit vector along the body axes specified in terms of the navigation axes. That means, the matrix $\boldsymbol{C}^k$ represents the rotation of the body frame with respect to the navigation frame at the time k (see Fig. 1). From this rotation the orientation of the sensor is deduced.

The orientation at the time k is the orientation at the time $k-1$ modified by the rotation that took place within the last δt seconds, represented in a matrix form as $\boldsymbol{A}^k$:

$$\boldsymbol{C}^k = \boldsymbol{C}^{k-1} \cdot \boldsymbol{A}^k, \tag{2}$$

being $\boldsymbol{A}^k$

$$\boldsymbol{A}^k = \boldsymbol{I} + \frac{\sin(\boldsymbol{\sigma})}{\boldsymbol{\sigma}} \cdot \boldsymbol{B}^k + \frac{1 - \cos(\boldsymbol{\sigma})}{\boldsymbol{\sigma}^2} \cdot \boldsymbol{B}^{k^2}, \tag{3}$$

where $\boldsymbol{\sigma} = |\boldsymbol{\omega}^k \delta t|$ and

$$\boldsymbol{B}^k = \begin{pmatrix} 0 & -\omega_z^k \delta t & \omega_y^k \delta t \\ \omega_z^k \delta t & 0 & -\omega_x^k \delta t \\ -\omega_y^k \delta t & \omega_x^k \delta t & 0 \end{pmatrix}. \tag{4}$$

In order to tackle the estimation of the biases of the gyroscope, a noise model is presented in the following. The biases are predicted using the presented model. The turn rate measurements $\boldsymbol{\omega}^k$ can be represented as

$$\boldsymbol{\omega}^k = \tilde{\boldsymbol{\omega}}^k + \boldsymbol{e}^k, \tag{5}$$

being $\tilde{\boldsymbol{\omega}}^k$ the error free turn rate and $\boldsymbol{e}^k$ the measurement error. The turn rate error can be decomposed into two errors

$$\boldsymbol{e}^k = \boldsymbol{b}^k + \boldsymbol{v}, \tag{6}$$

where $\boldsymbol{v}$ is the sensor noise that can be modeled as Gaussian white noise. To determine the biases error an auto-regressive model of order one (AR1) (Munoz Diaz et al., 2013) is chosen. The AR1 model is defined as

$$\hat{\boldsymbol{b}}^k = \boldsymbol{c} \cdot \boldsymbol{b}^{k-1} + \boldsymbol{n}. \tag{7}$$

The biases follow an exponentially correlated noise term defined in the AR1 model as the constant $\boldsymbol{c}$, which is equal to the term $e^{-\frac{1}{\tau}}$, where $\boldsymbol{\tau}$ is the correlation coefficient for each axis and $\boldsymbol{n}$ can be modeled as Gaussian white noise with standard deviation $\boldsymbol{\sigma_n}$ for each axis.

3.2 Update Stage

There are several updates that can be implemented to improve the orientation estimation. Usually the updates are signals directly measured by the sensors, but also pseudo-measurements can act as updates. The term pseudo-measurement refers to non-directly measured but computed signals. In the following, the most important updates will be summarized.

3.2.1 Absolute Gravity Update

During the walk, there are periods in which the acceleration due to the movement of the sensor is zero or quasi-zero. During these periods only the gravity acceleration is measured. In such case, the orientation angles roll and pitch can be extracted at the time k as follows:

$$\bar{\phi}^k = \arctan\left(\frac{\alpha_{\mathrm{y}}^k}{\alpha_{\mathrm{z}}^k}\right) \tag{8}$$

and

$$\bar{\theta}^k = \arctan\left(\frac{-\alpha_{\mathrm{x}}^k}{\sqrt{\alpha_{\mathrm{y}}^{k\,2} + \alpha_{\mathrm{z}}^{k\,2}}}\right). \tag{9}$$

The measurement vector $\boldsymbol{z}_{\mathrm{o}}^k$ of the Kalman filter at the time k can be written as:

$$\boldsymbol{z}_{\mathrm{o}}^k = [\bar{\phi}^k, \bar{\theta}^k]^T. \tag{10}$$

3.2.2 Differential Gravity Update

Likewise, within the periods of zero or quasi-zero acceleration, the acceleration at the current time can be computed applying the rotation of the last δt seconds, $\boldsymbol{A}^k$, to the acceleration measured at the previous time $\boldsymbol{\alpha}^{k-1}$ as follows:

$$\bar{\boldsymbol{\alpha}}^k = \boldsymbol{A}^k \cdot \boldsymbol{\alpha}^{k-1}. \tag{11}$$

The pseudo-measurement $\bar{\boldsymbol{\alpha}}^k$ is used as update. This update has been proposed in Renaudin and Combettes (2014). The measurement vector $\boldsymbol{z}_{\mathrm{o}}^k$ of the Kalman filter at the time k can be written as:

$$\boldsymbol{z}_{\mathrm{o}}^k = [\bar{\alpha}_{\mathrm{x}}^k, \bar{\alpha}_{\mathrm{y}}^k, \bar{\alpha}_{\mathrm{z}}^k]^T. \tag{12}$$

3.2.3 Absolute Magnetic Field Update

During the walk there are periods in which the measured magnetic field is constant or quasi-constant. At the beginning of the quasi-constant magnetic field period, the measured magnetic field is projected onto the navigation frame and chosen as reference $\bar{\boldsymbol{\mu}}_{\mathrm{r}}$. It is

assumed that, during quasi-constant magnetic field periods, the measured magnetic field does not change. Therefore, the reference magnetic field is used as pseudo-measurement for the update. This update has been proposed in Azfal et al. (2011) and further analyzed in Bancroft and Lachapelle (2012). The measurement vector $\boldsymbol{z}_{\mathrm{o}}^{k}$ of the Kalman filter at the time k can be written as:

$$\boldsymbol{z}_{\mathrm{o}}^{k} = [\bar{\mu}_{\mathrm{r_x}}, \bar{\mu}_{\mathrm{r_y}}, \bar{\mu}_{\mathrm{r_z}}]^{T}. \tag{13}$$

3.2.4 Differential Magnetic Field Update

Likewise, within these periods of constant or quasi-constant magnetic field, the magnetic field at the current time can be computed applying the rotation of the last δt seconds, $\boldsymbol{A}^{k}$, to the magnetic field measured at the previous time $\boldsymbol{\mu}^{k-1}$ as follows:

$$\bar{\boldsymbol{\mu}}^{k} = \boldsymbol{A}^{k} \cdot \boldsymbol{\mu}^{k-1}. \tag{14}$$

The pseudo-measurement $\bar{\boldsymbol{\mu}}^{k}$ is used as update. This update has been proposed in Zampella et al. (2012) and Azfal et al. (2011). The measurement vector $\boldsymbol{z}_{\mathrm{o}}^{k}$ of the Kalman filter at the time k can be written as:

$$\boldsymbol{z}_{\mathrm{o}}^{k} = [\bar{\mu}_{\mathrm{x}}^{k}, \bar{\mu}_{\mathrm{y}}^{k}, \bar{\mu}_{\mathrm{z}}^{k}]^{T}. \tag{15}$$

3.2.5 Absolute Compass Update

If the measured magnetic field is homogeneous, the yaw angle can be computed at each time k as follows:

$$\bar{\psi}^{k} = \arctan\left(\frac{-\mu_{\mathrm{h_x}}^{k}}{\mu_{\mathrm{h_y}}^{k}}\right) + \mathrm{D}, \tag{16}$$

being $\boldsymbol{\mu}_{\mathbf{h}_i}^{k}$ where $i = \{\mathrm{x,y}\}$ is the magnetic field intensity at the time k for the i-axis projected onto the horizontal plane. The declination angle, which is known for every location on the Earth, is represented by D. The measurement z_{o}^{k} of the Kalman filter at the time k can be written as:

$$z_{\mathrm{o}}^{k} = \bar{\psi}^{k}. \tag{17}$$

3.2.6 Zero Angular Rate Update

Within the periods where the sensor is not rotating, the turn rate measurements can be assumed to be zero. This assumption implies that any turn rate measured during these periods is due to errors, e.g., biases. This update has been proposed in Groves (2013). The measurement vector $\boldsymbol{z}_{\mathrm{o}}^{k}$ of the Kalman filter at the time k can be written as:

$$\boldsymbol{z}_{\mathrm{o}}^{k} = [0, 0, 0]^{T}. \tag{18}$$

4 Shoe-Mounted Inertial Positioning

Shoe-mounted positioning systems represent the first massively implemented positioning system for pedestrians. Shoe-mounted positioning is usually derived with the strapdown algorithm. The biomechanics of the foot allow performing re-calibrations at every step, thus limiting the rapidly growing positioning error. Back in 2005, Foxlin (2005) proposed to re-calibrate the strapdown algorithm for shoe-mounted systems performing Zero-velocity UPdaTes (ZUPT).

The strapdown algorithm is composed of two phases, namely orientation estimation and position estimation. Fig. 2 represents the block diagram of the strapdown algorithm.

The orientation estimation is performed as explained in Section 3, resulting in a direction cosine matrix $\boldsymbol{C}^k$ that represents the rotation of the body frame with respect to the navigation frame for each time k. The position estimation phase starts after the orientation is computed. The orientation is used to project the acceleration measurements onto the navigation frame.

$$\boldsymbol{\alpha}_{\mathrm{n}}^k = \boldsymbol{C}^k \cdot \boldsymbol{\alpha}^k. \tag{19}$$

Secondly, the gravity acceleration, $\boldsymbol{g}_{\mathrm{n}} = [0, 0, g]^T$, is subtracted from the projected acceleration. By doing so, the remaining acceleration corresponds only to the acceleration due to the movement of the body. Lastly, this remaining acceleration is integrated twice over time to compute the position. The algorithm strapdown requires an initial position p_0, an initial velocity v_0 and also an initial orientation. This is represented in the following equations:

$$\boldsymbol{v}_{\mathrm{n}}^k = \boldsymbol{v}_{\mathrm{n}}^{k-1} + \delta t \cdot (\boldsymbol{\alpha}_{\mathrm{n}}^k - \boldsymbol{g}_{\mathrm{n}}) \tag{20}$$

and

$$\boldsymbol{p}_{\mathrm{n}}^k = \boldsymbol{p}_{\mathrm{n}}^{k-1} + \delta t \cdot \boldsymbol{v}_{\mathrm{n}}^k, \tag{21}$$

being $\boldsymbol{p}^k$ the position at the time k, $\boldsymbol{v}$ the velocity at the time k, and δt the sampling time.

The shoe-mounted positioning is usually implemented using a Kalman filter, whose state vector $\boldsymbol{x}_{\mathrm{p}}$ is defined as follows:

$$\boldsymbol{x}_{\mathrm{p}}^k = [\boldsymbol{p}^k, \boldsymbol{v}^k, \boldsymbol{\Psi}^k, \boldsymbol{b}^k]^T, \tag{22}$$

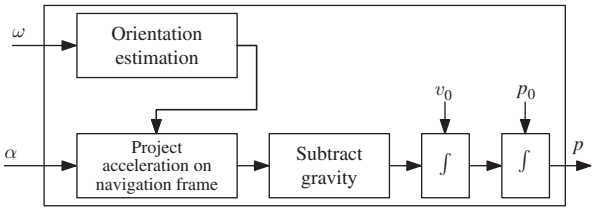

FIG. 2 Block diagram of the strapdown algorithm.

being $\boldsymbol{\Psi}^k$ the orientation at the time k and $\boldsymbol{b}^k$ the biases of the gyroscope at the time k. Also an error state Kalman filter is possible. The Kalman filter for shoe-mounted positioning systems is divided into two stages namely prediction and update. The equations described above represented by the block diagram of Fig. 2 represents the prediction stage. For error state Kalman filters, the equations described above do not form part of the filter, since the states consist of errors.

The aforementioned re-calibrations are performed during the update stage. The human gait cycle comprises eight phases (Streifeneder, 2016). Four of them can be observed using a foot-mounted sensor, i.e., the loading response, mid-stance, terminal stance, and swing as shown in Fig. 3.

In the case of shoe-mounted inertial positioning, the mid-stance is of high interest. The mid-stance phase is the period of the gait cycle when the foot is in contact with the ground. Fig. 4 represents the vertical acceleration measured by a shoe-mounted accelerometer. During the stance phases, indicated by the shadowed areas, the only acceleration measured by the shoe-mounted accelerometers is the gravity. Constant acceleration implies zero velocity, thus ZUPT corrections can be applied during these periods.

The stance phase detection is usually performed based on thresholds for the acceleration and turn rate (Foxlin, 2005). If both the acceleration and turn rate are within predefined thresholds during a minimum time, the stance phase is detected. The authors in Ruppelt et al. (2016) developed a stance phase detection based on a finite-state machine. In the latter, each phase of the human gait is a state of the finite-state machine. Such an approach can even detect the foot stance phase in challenging situations like walking the stairs.

Stance phase detection algorithms however, require these thresholds to be adapted to the particular inertial sensors, to the pedestrian or both. Furthermore, threshold-based algorithms perform optimally during walking on flat surfaces. In order to detect stance phases during other activities, e.g., walking stairs, a more sophisticated method is suggested by the authors in Ruppelt et al. (2016). The disadvantage of the latter is its complexity regarding both, design and implementation.

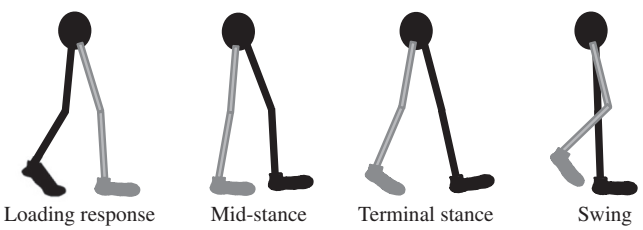

FIG. 3 Diagram of the gait phases visible using inertial sensors mounted on the right shoe *(grey leg)*.

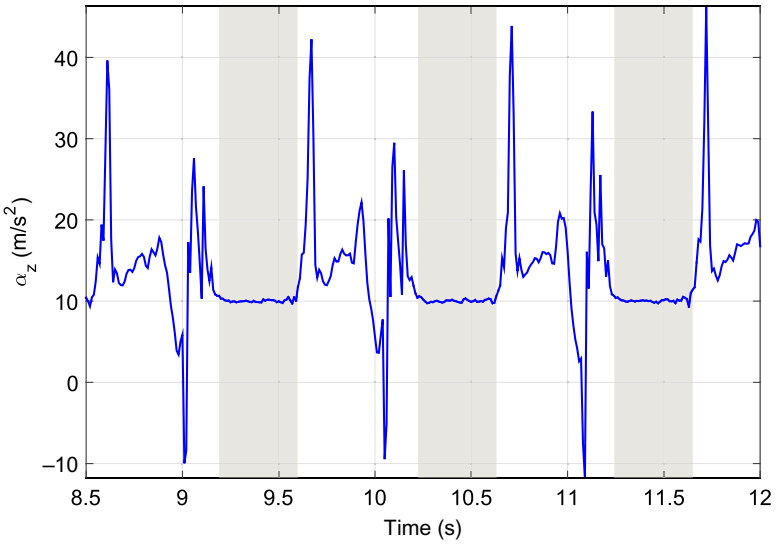

FIG. 4 Vertical acceleration measured by shoe-mounted accelerometers during three steps. The *shadowed areas* indicate the time when the foot is in mid-stance phase.

Upon detection of the stance phase, the states of the filter are updated with the ZUPT pseudo-measurement vector $\boldsymbol{z}_{\mathrm{p}}^{k}$ at the time k that can be written as:

$$\boldsymbol{z}_{\mathrm{p}}^{k} = [0, 0, 0]^{T}. \tag{23}$$

The use of ZUPT pseudo-measurements makes the error growth linear in time instead of cubic. The error accumulation, although linear, remains a challenge in pedestrian positioning based on shoe-mounted inertial sensors.

5 Non-shoe-Mounted Inertial Positioning

Non-shoe-mounted positioning systems are of high interest, because they can make use of the inertial sensors embedded in any wearable such as smart watch, smart glasses, and smart clothing among others. The error accumulated using these sensors cannot be mitigated with zero-velocity corrections, since the targeted body locations, i.e., head, wrist, etc. continuously move while walking. Therefore, in these cases the step&heading algorithm, represented in the block diagram of Fig. 5, is appropriate.

The step&heading algorithm is based on the following equations:

$$\begin{aligned} p_{\mathrm{x}}^{k} &= p_{\mathrm{x}}^{k-1} + s^{k} \cdot \cos(\psi^{k}), \\ p_{\mathrm{y}}^{k} &= p_{\mathrm{y}}^{k-1} + s^{k} \cdot \sin(\psi^{k}), \end{aligned} \tag{24}$$

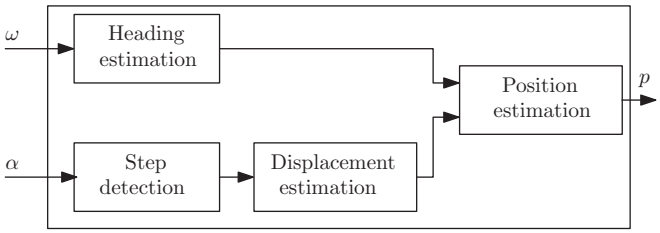

FIG. 5 Block diagram of the step&heading algorithm.

where p_x^k and p_y^k represent the position in the x- and y-axis at the time k, s^k stands for the step length at the time k and ψ^k is the heading of the pedestrian at the time k. Therefore, in order to compute the position of the pedestrian, two steps are necessary: the orientation estimation, to have the heading angle, and the displacement estimation.

The orientation estimation is carried out as described in Section 3. The different updates are not usually applied continuously, but only within particular periods, as explained in Section 3. From the complete orientation, usually only the heading angle ψ is used to compute the position of the pedestrian, as indicated in Eq. (24).

The step&heading algorithm is usually defined in 2D, as indicated in Eq. (24). However, for particular sensor locations it is possible to solve 3D positioning. In that case the position in the z-axis is as follows:

$$p_z^k = p_z^{k-1} + d_z^k, \tag{25}$$

where d_z^k represents the vertical displacement from the time $k-1$ to the time k. The authors in Munoz Diaz and Mendiguchia Gonzalez (2014) demonstrate that, if the inertial sensors are attached to the lower limb of the pedestrian, it is possible to differentiate between walking horizontally and climbing stairs by means of the orientation of the leg of the pedestrian. The information on the walking surface allows deriving the vertical displacement d_z.

The displacement estimation, being the step length or also the vertical displacement, is triggered every time a new step is detected, as shown in Fig. 5. The following subsections detail the step detection on horizontal surfaces, the step detection on stairs, the step length estimation and last but not least the vertical displacement estimation.

5.1 Step Detection on Horizontal Surfaces

The well known algorithm to detect steps is based on acceleration measurements. This algorithm is valid for all sensor locations. Fig. 6 shows the acceleration measured with the sensor introduced in the front pocket of the trousers. The dashed curve represents the norm of the acceleration $\|\alpha\|$ where the gravity has already been subtracted. A common procedure is to apply a low-pass filter (LPF) to this signal, in order to improve the performance regarding undetected steps and false detected steps. The LPF curve is shown

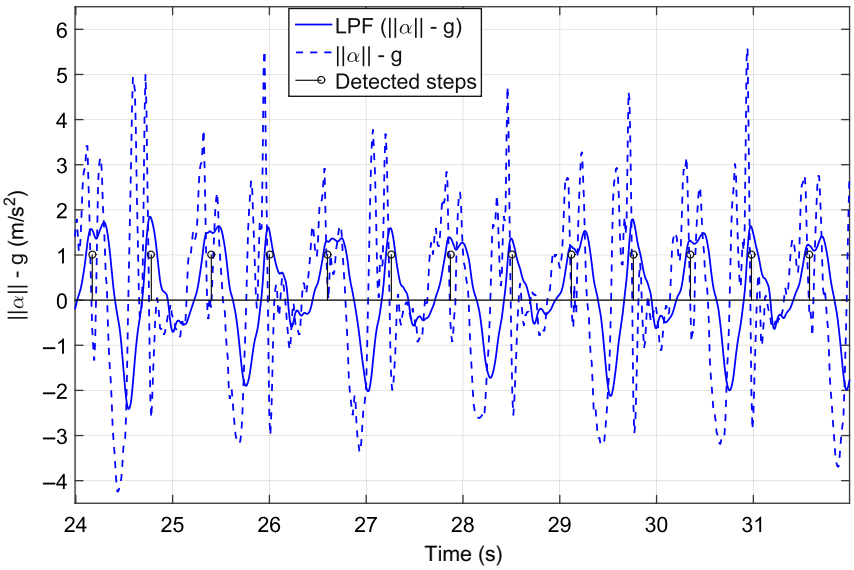

FIG. 6 The *dashed curve* represents the norm of the acceleration α with the gravity compensated, while the *solid curve* represents the low-pass filtered (LPF) acceleration. The detected steps are highlighted with *sticks*.

in solid and the detected steps are highlighted with sticks. In Munoz Diaz (2015), the performance of step detectors based on the norm of the acceleration and its low-pass filtered version has been analyzed. For horizontal surfaces, i.e., 2D walks, the false step detection rate decreases by using the filtered acceleration.

For some sensor locations, e.g., the lower limb, the step detection can also be performed using the pitch angle estimation, as suggested in Munoz Diaz and Mendiguchia Gonzalez (2014) and Xiao et al. (2014). Fig. 7 shows the pitch angle estimation for seven steps where the sensor has been introduced in the front pocket of the trousers. The detected steps are highlighted with sticks. In Munoz Diaz (2015), the performance of the step detector based on the pitch has been compared with the step detector based on the acceleration. The authors demonstrate that the step detection based on the pitch angle is more robust also for different walking speeds.

5.2 Step Detection on Stairs

Since the step&heading only based on inertial measurements is usually limited to horizontal displacements, i.e., 2D scenarios, the step detectors based on the acceleration do not offer reliable results when walking on stairs. The analysis carried out in Munoz Diaz (2015) for 3D scenarios shows that the undetected steps rate is high. However, the false detection rate is dramatically reduced by using the low-pass filtered acceleration. The authors in Munoz Diaz (2015) concluded that it is possible to successfully detect all steps

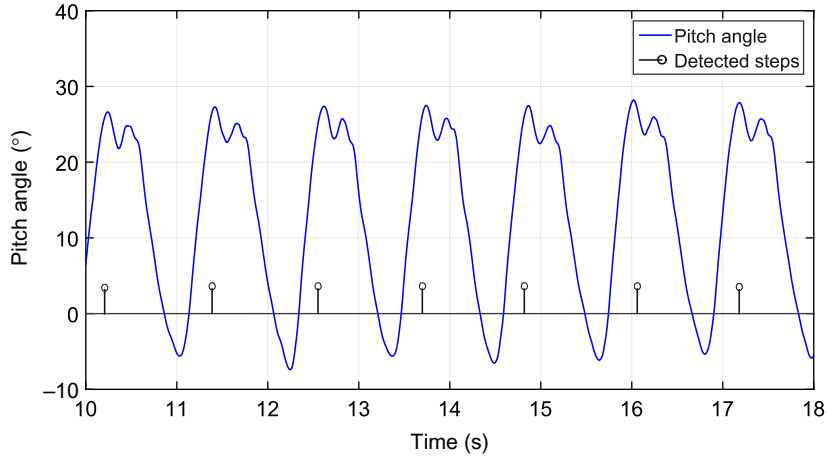

FIG. 7 The *curve* represents the pitch angle estimation over seven steps and the steps detected are highlighted with *sticks*.

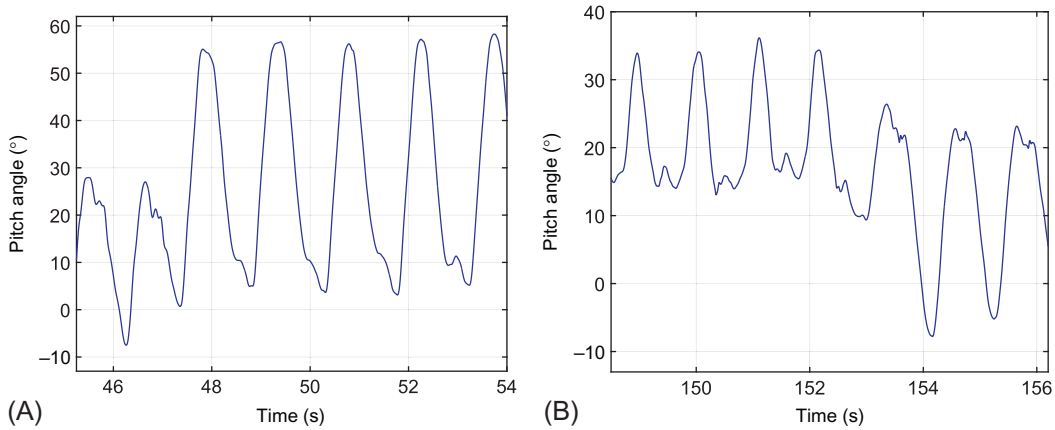

FIG. 8 (A) The pitch angle estimation when walking first two steps horizontally and then upstairs. (B) The pitch angle estimation when walking downstairs and the last three steps were taken walking horizontally.

while walking on stairs with the pitch-based step detector. Fig. 8 shows on the left side seven steps, where the first two steps were taken on an horizontal surface and the rest walking upstairs. The right side shows the pitch estimation during seven steps where the first four where taken walking downstairs and on an horizontal surface and the following three walking horizontally. The authors in Munoz Diaz (2015) show that detecting all steps is possible in 3D scenarios when using the pitch-based step detector. Additionally, it is possible to distinguish whether the pedestrian is walking horizontally, upstairs, or downstairs, which is the key to estimate the vertical displacement.

5.3 Step Length Estimation

The main current algorithms to compute the step length s^k at each time k can be classified depending on the sensor location, as specified in Alvarez et al. (2006) and Jahn et al. (2010).

If the sensor is attached to the body near the center of mass, two options exist:

- Based on a biomechanical model, where the kneeless biped is modeled as an inverted pendulum. The final estimation is scaled by a constant m that is calibrated for each user (Shih et al., 2012).

$$s^k = m \cdot \sqrt{2 \cdot L \cdot d_{z_p}^k - d_{z_p}^{k\,2}}, \tag{26}$$

  where $d_{z_p}^k$ represents the vertical displacement of the pelvis at the time k and L, the leg's length.
- Using an empirical relationship of the vertical acceleration and the step length (Jin et al., 2011; Goyal et al., 2011). The final estimation is scaled by a constant m that is calibrated for each user.

$$s^k = m \cdot \sqrt[4]{\alpha_{z_{\max}} - \alpha_{z_{\min}}}, \tag{27}$$

  where $\alpha_{z_{\max}}$ and $\alpha_{z_{\min}}$ are the maximum and minimum values of the vertical acceleration during each step.

If there are no restrictions on the sensor location on the human body (Shin et al., 2007, 2010; Gusenbauer et al., 2010; Renaudin et al., 2012, 2013), taking advantage of the relationship between step length, height of the user h, step frequency f_s^k at the time k and the calibration parameters (j, l, q) different for each user, the step length can be estimated as:

$$s^k = h \cdot (j \cdot f_s^k + l) + q. \tag{28}$$

In Munoz Diaz and Mendiguchia Gonzalez (2014), the step length estimator based on the pitch angle was presented. The authors assessed the relationship between the pitch amplitude and the step length with measurements recorded by 18 volunteers of different age, gender, height, and weight at different walking speeds. The authors propose a linear step length model based as follows:

$$s^k = j \cdot \Delta\theta_{\mathrm{H}}^k + l, \tag{29}$$

where $\Delta\theta_{\mathrm{H}}^k$ represents the pitch amplitude in horizontal surfaces at the time k. The parameters (j, l) can be universal or personalized for each pedestrian.

The authors in Munoz Diaz (2015) show an analysis comparing the step length estimator based on the step frequency and based on the pitch angle for a sensor introduced in the front pocket of the trousers. The results reveal that, for normal and constant walking speed, both estimators offer similar performance. However, for very low walking speed

including stops and for high walking speeds, the detector based on the pitch angle offers more accurate results than the detector based on the step frequency.

5.4 Vertical Displacement Estimation

The authors in Munoz Diaz (2015) estimate, for the first time, the vertical displacement in a step&heading algorithm using only inertial sensors. This is possible thanks to the pitch angle estimation that allows identifying whether the pedestrian is walking horizontally or climbing stairs. The pitch angle estimation allows also distinguishing between walking downstairs and upstairs. In order to estimate the vertical displacement d_{v}, the authors carried out a set of experiments with the objective of finding a relationship between the pitch angle and the height of the steps of the staircase. The results show that there is a relationship between the amplitude of the pitch angle and the height of the steps. The authors propose a linear model that relates these two variables for walking downstairs and upstairs as follows:

$$\begin{aligned} d_{\mathrm{v_U}}^k &= j \cdot \Delta\theta_{\mathrm{U}}^k + l, \\ d_{\mathrm{v_D}}^k &= q \cdot \Delta\theta_{\mathrm{D}}^k + w, \end{aligned} \tag{30}$$

where $d_{\mathrm{v_U}}^k$ and $d_{\mathrm{v_D}}^k$ are the estimated vertical displacement for up and downstairs, respectively, at the time stamp k. $\Delta\theta_{\mathrm{U}}^k$ and $\Delta\theta_{\mathrm{D}}^k$ represent the pitch amplitude for steps up and down, respectively, at the time stamp k. The parameters (j, l, q, w) can be universal or personalized for each pedestrian.

The presented model is valid to estimate the height of the steps up and down of the vast majority of the staircases that can be found in every building, because it assumes a standard depth and focuses on the height of the step. Thus, the horizontal displacement is assumed.

Fig. 9 shows a 3D trajectory corresponding to a walk recorded in the German museum in Munich with the sensor introduced in the front pocket of the trousers and using only inertial sensors. The walk starts at (0, 0, 0) and at the point (90, −20, 0) the pedestrian takes the stairs until the first floor. Then the pedestrian walks a round on the first floor and takes

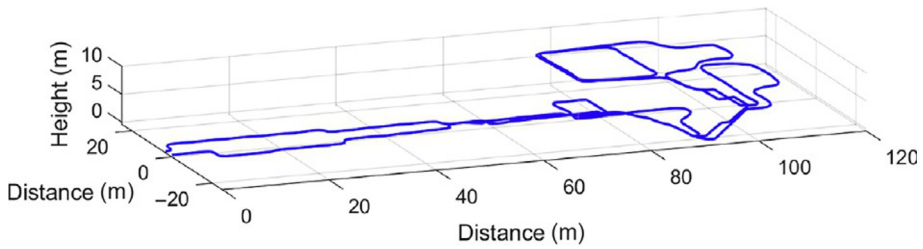

FIG. 9 The *curve* shows the 3D trajectory estimated using only inertial sensors introduced in the front pocket of the trousers.

the stairs to the second floor. After some rounds on the second floor the pedestrian walks downstairs two floors and comes back to the initial position.

The algorithm proposed by the authors assumes that the height of all steps of the staircase is the same, i.e., v_U and v_D are equal. Thus, the algorithm gathers data when walking up and downstairs and the height of the steps of the staircase is estimated with the average of the pitch amplitude of all steps up and down using Eq. (30).

6 Drift Reduction Methods

Regarding pedestrian inertial navigation systems using medium- and low-cost MEMS sensors, the accumulated error in the yaw angle estimation is still an unsolved issue. This error, commonly called drift, should be computed and used to prevent positioning errors.

The authors in Munoz Diaz et al. (2017) concluded that the drift error is mainly composed of biases, particularly the bias of the z-axis gyroscope. The biases of the x- and y-axes gyroscopes can be estimated through the gravitational field, as assessed in Munoz Diaz et al. (2017). Therefore, the error in roll and pitch angles can be corrected with the estimation of the x- and y-axes biases. On the contrary, the yaw angle suffers from ever growing errors that mainly arise from a poor estimation of the bias of the z-axis gyroscope (Munoz Diaz et al., 2017).

Additionally, there is an accumulating error in the vertical axis, i.e., height error. This severe error is in most of the cases mitigated with the use of barometers. However, there are also solutions for only inertial-based systems that are described in this section.

6.1 Heuristic Drift Elimination Algorithms

Heuristic drift elimination algorithms assume that pedestrians walk on a straight line in the building in directions which are parallel to the outer walls of the building. If the pedestrian does not move on a straight line, these corrections are suspended (Borenstein and Ojeda, 2010). After the first heuristic drift elimination algorithm was published, many authors in the literature have proposed similar ideas or improvements, such as coping with complex buildings including curved corridors or wide areas not restricted by corridors (Abdulrahim et al., 2010, 2012; Jimenez et al., 2011).

Additionally, the heuristic drift elimination has been suggested in combination with other heading corrections such as zero angular rate updates and magnetic measurements (Jimenez et al., 2010, 2012). The combination with available maps has also been proposed to restrict the possible heading angles by taking into account the walls of the buildings (Aggarwal et al., 2011; Pinchin et al., 2012). The high nonlinearities of the maps force the use of particle filters that weight the particles according to the similarity of their heading with the direction of the walls. The main drawback of these approaches is that previous knowledge is necessary, e.g., the map or the shape of the corridors.

6.2 SLAM-Based Algorithms

A suitable solution to drift reduction is the use of the simultaneous localization and mapping (SLAM) algorithm, which has been used for decades in robotics. The SLAM algorithm simultaneously generates a map of the desired landmarks and locates the user/robot within this map. These landmarks can be detected with any sensor, such as a laser scanner or a camera. The automatic vacuum cleaner, for example, generates a map of the room and locates itself within this map where the interesting landmarks, i.e., sofa, table, doors are included.

The SLAM algorithm has also been adapted to pedestrian navigation aiming at reducing the drift error. In order for the SLAM algorithm to successfully reduce the drift, a re-visit is necessary. That means, the pedestrian detects landmarks during the trajectory and, when part of the trajectory is re-visited, the landmark is again detected. The same landmark detected twice is an indicative of being again at the same position, therefore, corrections can be applied.

Commonly a particle filter is used that generates particles that move with different errors. When landmarks are re-visited, all particles are weighted depending on the landmarks position. Thus, particles that followed a trajectory with the current drift are high weighted, because they most likely correspond to the detected position. In Robertson et al. (2009), the 2D space is divided into a grid of uniform and adjacent hexagons, which can be considered as landmarks. When the same hexagons are re-visited the aforementioned corrections are carried out. The same procedure is applied for 3D trajectories but dividing the volume into hexagonal prisms with eight faces (Garcia Puyol et al., 2014). This procedure can also be applied if the hexagons are identified by the magnetic field intensity (Robertson et al., 2013). The main drawback of these algorithms is the complexity and processing time to manage the numerous hexagons or hexagonal prisms.

In Hardegger et al. (2012), the proposed landmarks are some location-related activities carried out by the pedestrian, such as sitting, lying, or opening doors. Based on the assumption that these activities are always performed at the same place, their repeated detection leads to the aforementioned corrections. The main drawback of these methods is that the heading estimation is not explicitly corrected, just corrections on the position are applied.

6.3 Multi-inertial Sensor Fusion

Multi-inertial sensor fusion combines two or more inertial sensors to reduce the drift in inertial positioning systems. Multi-inertial sensor fusion algorithms can be classified into two types: loose coupling and tight coupling.

Loose coupling algorithms combine the output of different inertial positioning systems. The aim is to generate a combined position estimation with less drift than the individual position estimations. The authors in Bousdar Ahmed and Munoz Diaz (2017) propose a loose coupling algorithm to combine the outputs of a shoe-mounted and a pocket-mounted inertial sensors. The so-called smart update approach is followed, i.e., the

individual position estimations are combined favoring automatically the one containing less drift. A novel metric, the quality factor, is proposed to seamlessly identify which position estimation contains less drift.

Tight coupling algorithms target drift reduction by combining the raw data from two or more inertial sensors. On the one hand, inertial sensor arrays can be used to process all individual acceleration and turn rate measurements. In Skog et al. (2016), a maximum likelihood estimator combines the measurements from an array and the authors state that the information gained is proportional to the square of the array dimension. On the other hand, human biomechanics can also be used to reduce the drift. The body mounted sensors in Ahmadi et al. (2015) are combined to reduce the drift in a gait monitoring system. The authors use a kinematic leg model to ensure that the motion is coherent with the biomechanical behavior of the leg.

6.4 Landmark-Based Algorithms

In Millonig and Schechtner (2007), a study has been carried out concluding that landmarks play an important role for pedestrian navigation, therefore, it is recommendable to develop methods to include landmarks information in pedestrian navigation systems.

One of the most intuitive ways of detecting landmarks during the trajectory is using visual information. The chosen landmarks are tracked over time in order to use this motion to constrain the drift. In Griesbach et al. (2014), a stereo vision camera is used to extract the optical information of the landmarks. The heuristic drift elimination algorithms can also be seen as landmark-based algorithms, since the manmade straight corridors can be interpreted as landmarks. The main difference is that the landmarks of the heuristic drift elimination algorithms do not need to be tracked over time.

In Jimenez R. et al. (2011), an algorithm that makes use of detected ramps in buildings for correcting the drift is presented. In the article, foot-mounted inertial sensors are used and the position of the ramps of the target building is previously known. Ramps are detected through the slope of the terrain and corrections of the position of the pedestrian are applied. However, this approach does not compute the drift value. Therefore, although the position is corrected, the proposed approach does not bind the error of the yaw angle.

In Munoz Diaz et al. (2017) and Munoz Diaz and Caamano (2017), the authors propose the use of landmarks to compensate the drift error. The proposed landmarks are corners and stairs, thus, plentiful in indoor environments. These landmarks are seamlessly detected using only inertial sensors. The algorithm is based on re-visiting these landmarks in order to perform corrections. The trajectory of the landmark during the re-visit can be fully or partially overlapped or even with no overlap. The novelty of this contribution relies on computing the drift value. This accumulated drift is fed back to the orientation filter. This approach allows the yaw angle to be corrected and also prevent future positioning errors due to a drifted yaw angle estimation. Additionally, position corrections are also carried out. The authors recommend, depending on the positioning system requirements, to

perform these corrections online, while the landmarks are re-visited, or offline, computing the overall drift value and using it to postprocess the recorded data.

6.5 Height Error Correction

The error in the height computation is the source of the confusion between different floors. This error is usually mitigated using barometers. The barometer sensor relates the change of height with the atmospheric pressure changes. The height error is mainly affecting the shoe-mounted inertial systems, because the step&heading approach is usually 2D defined.

There are several approaches for only inertial-based systems using medium- and low-cost MEMS sensors to correct the height error. The authors in Munoz Diaz et al. (2018) use the pitch angle of the foot to identify if the pedestrian is walking on horizontal surfaces or climbing stairs. The authors in Abdulrahim et al. (2012) apply an empirical threshold to assume that the user is walking horizontally and apply height corrections. These corrections act keeping the height at the same value, when the pedestrian is walking horizontally and only during the mid-stance phase (see Fig. 4). The authors in Ruppelt et al. (2016) apply also height constraints based on a finite state machine step detector.

7 Conclusions

In this chapter a review of the methods applied for pedestrian positioning using inertial sensors has been presented. Pedestrian inertial positioning is usually derived in two different ways depending on the location of the sensor on the human body: (i) for shoe-mounted sensors the strapdown algorithm is used, due to the possibility of perform re-calibrations at every step; (ii) for the rest of body locations the step&heading algorithm is preferred.

The big advantage of medium- and low-cost MEMS inertial sensors relies on their low price, small size, and widespread. Additionally, inertial positioning constitutes an infrastructure-less positioning system. Their clear disadvantage, however, is the remaining drift error on the estimated positioning.

There are many publications tackling the compensation of the drift error resulting when using inertial sensors. Drift affects inertial positioning disregarding the body location where the sensor is mounted on. Nowadays the trend is clearly pointing at sensor fusion. That means, combining the information of all sensors available. Especially recommended is the fusion with satellite and radio positioning systems. The piloting method does not suffer from drift, unlike the dead-reckoning method that propagates and accumulates error over time. This chapter, however, is focused on inertial sensors, thus, a review of the latest drift reduction methods using only inertial sensors is provided.

However, the current research on pedestrian inertial positioning is slowly approaching a static stage. While the latest proposals on sensor fusion and drift reduction algorithms greatly contribute to a more accurate positioning, the fact is that the drift error is low-bounded by the sensor technology. The breakthrough will be driven by the next

generation of compact inertial sensors. In future, the inertial pedestrian dead-reckoning performed with the strapdown algorithm will be possible disregarding the body location where the sensor is mounted on. The next generation of high-quality compact inertial sensors will eliminate the current strong need of performing constant re-calibrations by offering a more steady bias stability.

References

Abdulrahim, K., Hide, C., Moore, T., Hill, C., 2010. Aiding MEMS IMU with building heading for indoor pedestrian navigation. In: Ubiquitous Positioning Indoor Navigation and Location Based Service (UPINLBS). IEEE.

Abdulrahim, K., Hide, C., Moore, T., Hill, C., 2012. Using constraints for shoe mounted indoor pedestrian navigation. R. Inst. Navig. 65, 15–28.

Aggarwal, P., Thomas, D., Borenstein, J., Ojeda, L., 2011. Map matching and heuristic elimination of gyro drift for personal navigation systems in GPS-denied conditions. J. Meas. Sci. Technol. 22.

Ahmadi, A., Destelle, F., Monaghan, D., Moran, K., O-Connor, N.E., Unzueta, L., Linaza, M.T., 2015. Human gait monitoring using body-worn inertial sensors and kinematic modelling. In: 2015 IEEE SENSORS. IEEE. https://doi.org/10.1109/icsens.2015.7370310.

Alvarez, D., González, R.C., López, A., Alvarez, J.C., 2006. Comparison of step length estimators from wearable accelerometer devices. In: 28th Annual International Conference of the IEEE Engineering in Medicine and Biology Society, 2006. EMBS'06. IEEE, pp. 5964–5967.

Azfal, M.H., Renaudin, V., Lachapelle, G., 2011. Use of Earth's magnetic field for mitigating gyroscope errors regardless of magnetic perturbation. Sensors 11, 11390–11414.

Bancroft, J.B., Lachapelle, G., 2012. Use of magnetic quasi static field (QSF) updates for pedestrian navigation. In: IEEE/ION Position Location and Navigation Symposium (PLANS).

Beauregard, S., Widyawan, Klepal, M., 2008. Indoor PDR performance enhancement using minimal map information and particle filters. In: Proceedings of the IEEE/ION Position Location and Navigation Symposium (PLANS) 2008, Monterey, USA.

Beroulle, V., Bertrand, Y., Latorre, L., Nouet, P., 2003. Monolithic piezoresistive CMOS magnetic field sensors. Sens. Actuators A: Phys. 103 (1), 23–32. https://doi.org/10.1016/S0924-4247(02)00317-5. http://www.sciencedirect.com/science/article/pii/S0924424702003175.

Borenstein, J., Ojeda, L., 2010. Heuristic drift elimination for personnel tracking systems. R. Inst. Navig. 63, 591–606.

Bousdar Ahmed, D., Munoz Diaz, E., 2017. Loose coupling of wearable-based INSs with automatic heading evaluation. Sensors 17, 2534. https://doi.org/10.3390/s17112534. http://www.mdpi.com/1424-8220/17/11/2534.

Bousdar, D., Munoz Diaz, E., Kaiser, S., 2016. Performance comparison of foot- and pocket-mounted inertial navigation systems. In: 7th International Conference on Indoor Positioning and Indoor Navigation, 4–7 October, 2016, Madrid, Spain.

Diez, L.E., Alfonso Bahillo, A., Bataineh, S., Masegosa, A.D., Perallos, A., 2016. Enhancing improved heuristic drift elimination for wrist-worn PDR systems in buildings. In: 2016 IEEE 84th Vehicular Technology Conference (VTC-Fall), pp. 1–5.

Do, T.N., Liu, R., Yuen, C., Zhang, M., Tan, U.X., 2016. Personal dead reckoning using IMU mounted on upper torso and inverted pendulum model. IEEE Sens. J. 16 (21), 7600–7608.

Foxlin, E., 2005. Pedestrian tracking with shoe-mounted inertial sensors. IEEE Comput. Graph. Appl. 25 (6), 38–46.

Garcia Puyol, M., Bobkov, D., Robertson, P., Jost, T., 2014. Pedestrian simultaneous localization and mapping in multistory buildings using inertial sensors. IEEE Trans. Intell. Trans. Syst. 15, 1714–1727.

Goyal, P., Ribeiro, V.J., Saran, H., Kumar, A., 2011. Strap-down pedestrian dead-reckoning system. In: 2011 International Conference on Indoor Positioning and Indoor Navigation (IPIN). IEEE, pp. 1–7.

Griesbach, D., Baumbach, D., Zuev, S., 2014. Stereo-vision-aided inertial navigation for unknown indoor and outdoor environments. In: IEEE International Conference on Indoor Positioning and Indoor Navigation (IPIN). IEEE, pp. 709–716.

Groves, P.D., 2013. Principles of GNSS, inertial, and multisensor integrated navigation systems, second ed. Artech House. ISBN 9781608070053.

Gu, Y., Lo, A., Niemegeers, I., 2009. A survey of indoor positioning systems for wireless personal networks. IEEE Commun. Surv. Tutorials 11 (13–32), 1281–1293.

Gusenbauer, D., Isert, C., Krosche, J., 2010. Self-contained indoor positioning on off-the-shelf mobile devices. In: 2010 International Conference on Indoor Positioning and Indoor Navigation (IPIN). IEEE, pp. 1–9.

Hardegger, M., Roggen, D., Mazilu, S., Troster, G., 2012. ActionSLAM: using location-related actions as landmarks in pedestrian SLAM. In: IEEE International Conference on Indoor Positioning and Indoor Navigation (IPIN). IEEE.

Harle, R., 2013. A survey of indoor inertial positioning systems for pedestrians. IEEE Commun. Surv. Tutorials 15 (3), 1281–1293.

Jahn, J., Batzer, U., Seitz, J., Patino-Studencka, L., Gutiérrez Boronat, J., 2010. Comparison and evaluation of acceleration based step length estimators for handheld devices. In: 2010 International Conference on Indoor Positioning and Indoor Navigation (IPIN). IEEE, pp. 1–6.

Jimenez, A.R., Seco, F., Prieto, J.C., Guevara, J., 2010. Indoor pedestrian navigation using an INS/EKF framework for yaw drift reduction and a foot-mounted IMU. In: 7th Workshop on Positioning Navigation and Communication (WPNC). IEEE, pp. 135–143.

Jimenez, A.R., Seco, F., Zampella, F., Prieto, J.C., 2011. Improved heuristic drift elimination (iHDE) for pedestrian navigation in complex buildings. In: IEEE International Conference on Indoor Positioning and Indoor Navigation (IPIN). IEEE, pp. 1–8.

Jimenez, A.R., Seco, F., Zampella, F., Prieto, J.C., Guevara, J., 2012. Improved heuristic drift elimination with magnetically-aided dominant directions (MiHDE) for pedestrian navigation in complex buildings. J. Locat. Based Serv. 6, 186–210.

Jimenez A.R., Seco, F., Zampella, F., Prieto, J.C., Guevara, J., 2011. PDR with a foot-mounted IMU and ramp detection. Sensors 11, 9393–9410.

Jin, Y., Toh, H.S., Soh, W.S., Wong, W.C., 2011. A robust dead-reckoning pedestrian tracking system with low cost sensors. In: 2011 IEEE International Conference on Pervasive Computing and Communications (PerCom). IEEE, pp. 222–230.

Kaiser, S., Khider, M., Garcia Puyol, M., Bruno, L., Robertson, P., 2015. Map aided indoor navigation. In: Karimi, H. (Ed.), Indoor Wayfinding and Navigation. Taylor and Francis, pp. 107–140.

Krach, B., Robertson, P., 2008. Cascaded estimation architecture for integration of foot-mounted inertial sensors. In: Proceedings of the IEEE/ION Position Location and Navigation Symposium (PLANS) 2008, Monterey, USA.

Lenz, J., Edelstein, S., 2006. Magnetic sensors and their applications. IEEE Sens. J. 6 (3), 631–649. https://doi.org/10.1109/JSEN.2006.874493.

Liu, H., Darabi, H., Banerjee, P., Liu, J., 2007. Survey of wireless indoor positioning techniques and systems. IEEE Trans. Syst. Man Cybern. C: Appl. Rev. 37 (6), 1067–1080.

Millonig, A., Schechtner, K., 2007. Developing landmark-based pedestrian-navigation systems. IEEE Trans. Intell. Transp. Syst. 8 (1), 43–49.

Munoz Diaz, E., 2015. Inertial pocket navigation system: unaided 3D positioning. Sensors 15, 9156–9178. https://doi.org/10.3390/s150409156. http://www.mdpi.com/1424-8220/15/4/9156.

Munoz Diaz, E., Caamano, M., 2017. Landmark-based online drift compensation algorithm for inertial pedestrian navigation. In: IEEE International Conference on Indoor Positioning and Indoor Navigation (IPIN). IEEE.

Munoz Diaz, E., Mendiguchia Gonzalez, A.L., 2014. Step detector and step length estimator for an inertial pocket navigation system. In: IEEE International Conference on Indoor Positioning and Indoor Navigation (IPIN). IEEE.

Munoz Diaz, E., Heirich, O., Khider, M., Robertson, P., 2013. Optimal sampling frequency and bias error modeling for foot-mounted IMUs. In: IEEE International Conference on Indoor Positioning and Indoor Navigation (IPIN). IEEE.

Munoz Diaz, E., Mendiguchia Gonzalez, A.L., de Ponte Müller, F., 2014. Standalone inertial pocket navigation system. In: IEEE/ION Position Location and Navigation Symposium (PLANS). IEEE.

Munoz Diaz, E., Caamano, M., Fuentes Sanchez, F.J., 2017. Landmark-based drift compensation algorithm for inertial pedestrian navigation. Sensors 17, 1555. https://doi.org/10.3390/s17071555. http://www.mdpi.com/1424-8220/17/7/1555.

Munoz Diaz, E., de Ponte Müller, F., García Domínguez, J.J., 2017. Use of the magnetic field for improving gyroscopes' biases estimation. Sensors 17, 832. https://doi.org/10.3390/s17040832. http://www.mdpi.com/1424-8220/17/4/832.

Munoz Diaz, E., Kaiser, S., Bousdar Ahmed, D., 2018. Height error correction for shoe-mounted inertial sensors exploiting foot dynamics. Sensors 18, 888. https://doi.org/10.3390/s18030888. http://www.mdpi.com/1424-8220/18/3/888.

Pinchin, J., Hide, C., Moore, T., 2012. A particle filter approach to indoor navigation using a foot-mounted inertial navigation system and heuristic heading information. In: IEEE International Conference on Indoor Positioning and Indoor Navigation (IPIN). IEEE, pp. 1–10.

Renaudin, V., Combettes, C., 2014. Magnetic, acceleration fields and gyroscope quaternion (MAGYQ)-based attitude estimation with smartphone sensors for indoor pedestrian navigation. Sensors 14, 22864–22890.

Renaudin, V., Susi, M., Lachapelle, G., 2012. Step length estimation using handheld inertial sensors. Sensors 12 (7), 8507–8525.

Renaudin, V., Demeule, V., Ortiz, M., 2013. Adaptive pedestrian displacement estimation with a smartphone. In: International Conference on Indoor Positioning and Indoor Navigation, pp. 916–924.

Robertson, P., Angermann, M., Krach, B., 2009. Simultaneous localization and mapping for pedestrians using only foot-mounted inertial sensors. In: International Conference on Ubiquitous Computing, pp. 93–96.

Robertson, P., Frassl, M., Angermann, M., Doniec, M., Julian, B.J., Garcia Puyol, M., Khider, M., Lichtenstern, M., Bruno, L., 2013. Simultaneous localization and mapping for pedestrians using distortions of the local magnetic field intensity in large indoor environments. In: IEEE International Conference on Indoor Positioning and Indoor Navigation (IPIN). IEEE, pp. 1–10.

Ruppelt, J., Kronenwett, N., Scholz, G., Trommer, G.F., 2016. High-precision and robust indoor localization based on foot-mounted inertial sensors. In: 2016 IEEE/ION Position, Location and Navigation Symposium (PLANS), pp. 67–75. https://doi.org/10.1109/PLANS.2016.7479684.

Shin, S.H., Park, C.G., Kim, J.W., Hong, H.S., Lee, J.M., 2007. Adaptive step length estimation algorithm using low-cost MEMS inertial sensors. In: Sensors Applications Symposium, 2007. SAS'07. IEEE, pp. 1–5.

Shin, S.H., Lee, M.S., Park, C.G., Hong, H.S., 2010. Pedestrian dead reckoning system with phone location awareness algorithm. In: 2010 IEEE/ION Position Location and Navigation Symposium (PLANS). IEEE, pp. 97–101.

Shih, W.Y., Chen, L.Y., Lan, K.C., 2012. Estimating walking distance with a smart phone. In: 2012 Fifth International Symposium on Parallel Architectures, Algorithms and Programming (PAAP). IEEE, pp. 166–171.

Skog, I., Nilsson, J.O., Handel, P., Nehorai, A., 2016. Inertial sensor arrays, maximum likelihood, and Cramér-Rao bound. IEEE Trans. Signal Process. 64 (16), 4218–4227. https://doi.org/10.1109/tsp.2016.2560136.

Streifeneder, 2016. The eight phases of human gait cycle. https://www.streifeneder.com/downloads/o.p./400w43_e_poster_gangphasen_druck.pdf.

Wagner, J.F., Wieneke, T., 2003. Integrating satellite and inertial navigation—conventional and new fusion approaches. Control Eng. Pract. 11 (5), 543–550.

Windau, J., Itti, L., 2016. Walking compass with head-mounted IMU sensor. In: 2016 IEEE International Conference on Robotics and Automation (ICRA), pp. 5542–5547.

Woodman, O.J., 2007. An introduction to inertial navigation. Tech. Rep., University of Cambridge. Computer Laboratory, uCAM-CL-TR-696. ISSN 1476-2986.

Woodman, O., Harle, R., 2008. Pedestrian localisation for indoor environments. In: Proceedings of UbiComp 2008, Seoul, South Korea.

Xiao, Z., Wen, H., Markham, A., Trigoni, N., 2014. Robust pedestrian dead reckoning (R-PDR) for arbitrary mobile device placement. In: IEEE International Conference on Indoor Positioning and Indoor Navigation (IPIN). IEEE.

Zampella, F., Khider, M., Robertson, P., Jimenez, A., 2012. Unscented Kalman filter and magnetic angular rate update (MARU) for an improved pedestrian dead-reckoning. In: IEEE/ION Position Location and Navigation Symposium (PLANS). IEEE.